A Switched-Coupling-Capacitor Equalizer for Series-Connected Battery Strings

Yunlong Shang, *Student Member, IEEE*, Bing Xia, *Student Member, IEEE*, Fei Lu, *Student Member, IEEE*, Chenghui Zhang, *Member, IEEE*, Naxin Cui, *Member, IEEE*, and Chunting Chris Mi, *Fellow, IEEE*

***Abstract*—Due to the low cost, small size, and easy control, the switched-capacitor (SC) equalizer is promising among all types of active cell balancing methods. However, the balancing speed is generally slow and the balancing efficiency is seriously low when the SC equalizer is applied into a long battery string. Therefore, an automatic switched-coupling-capacitor equalizer (SCCE) is proposed, which can realize the any-cells-to-any-cells equalization for a battery string. Only two switches and one capacitor are required for each battery cell. All MOSFETs are controlled by one pair of complementary pulse width modulation signals, and energy can be automatically and directly delivered from any higher voltage cells to any lower voltage ones without the need of cell monitoring circuits, leading to a high balancing efficiency and speed independent of the cell number and the initial cell voltages. Contrary to the conventional equalizers using additional components for the equalization among modules, the proposed equalizer shares a single converter for the equalization among cells and modules, resulting in smaller size and lower cost. A prototype for four lithium battery cells is implemented, and an experimental comparison between the proposed SCCE and the conventional SC equalizer is presented. Experimental results show the proposed topology exhibits a substantially improved balancing performance, and the measured peak efficiency is 92.7%.**

***Index Terms*—Battery equalizers, battery management systems, electric vehicles (EVs), modularization, switched coupling capacitors (SCCs).**

Manuscript received September 2, 2016; revised November 1, 2016; accepted November 28, 2016. Date of publication December 9, 2016; date of current version May 9, 2017. This work was supported in part by the Major Scientific Instrument Development Program of the National Natural Science Foundation of China under Grant 61527809, in part by the Key Project of National Natural Science Foundation of China under Grant 61633015, Nanjing Golden Dragon Bus Co., Ltd., in part by the U.S. Department of Energy under the Graduate Automotive Technology Education Center program, and in part by the China Scholarship Council. Recommended for publication by Associate Editor O. Trescases.

Y. Shang is with the School of Control Science and Engineering, Shandong University, Shandong 250061, China, and also with the Department of Electrical and Computer Engineering, San Diego State University, San Diego, CA 92182 USA (e-mail: shangyunlong@mail.sdu.edu.cn).

B. Xia is with the Department of Electrical and Computer Engineering, San Diego State University, San Diego, CA 92182 USA, and also with the Department of Electrical and Computer Engineering, University of California San Diego, CA 92093 USA (e-mail: bixia@eng.ucsd.edu).

F. Lu is with the Electrical Engineering and Computer Science Department, University of Michigan, Ann Arbor, MI 48109 USA, and also with the Department of Electrical and Computer Engineering, San Diego State University, San Diego, CA 92182 USA (e-mail: feilu@umich.edu).

C. Zhang and N. Cui are with the School of Control Science and Engineering, Shandong University, Jinan, 250061, China (e-mail: zchui@sdu.edu.cn; cuinx@sdu.edu.cn).

C. C. Mi is with the Department of Electrical and Computer Engineering, San Diego State University, San Diego, CA 92182 USA (e-mail: cmi@sdsu.edu).

Color versions of one or more of the figures in this paper are available online at http://ieeexplore.ieee.org.

Digital Object Identifier 10.1109/TPEL.2016.2638318

I. Introduction

NOWADAYS, rechargeable batteries are widely applied in uninterruptible power supplies, artificial satellites, and electric vehicles as energy storage systems [1]. Due to the high energy density, low self-discharge rate, and no memory effect, lithium battery (i.e., lithium-ion, lithium polymer, or lithium iron phosphate ($LiFePO_4$) battery) has been regarded as one of the most attractive rechargeable batteries [2]. However, the terminal voltage of a single lithium battery cell is usually low, e.g., 3–4.2 V for lithium-ion battery cells and 2–3.65 V for $LiFePO_4$ battery cells [3]–[4]. Generally, in order to meet the load voltage and power requirements, lithium battery cells are usually connected in parallel and series to construct a battery pack [5]–[6]. Nevertheless, there are slight differences in terms of capacity, internal resistance, and voltage among cells, which will be enlarged as the battery pack ages [7]. Lithium batteries cannot be overcharged, which may lead to explosion or fire, and cannot be overdischarged, which may degrade the characteristics of batteries [7]. As a result, charging or discharging must be interrupted when any cell in the battery pack reaches its cutoff voltage, which does not utilize efficiently the energy storage potential of the battery pack [7]. Therefore, battery balancing is mandatory for series-connected battery packs to maximize the available operating range and to extend the battery life.

Many balancing circuits have been proposed during the last few years, which can be classified into two groups: the passive equalizers [7]–[8] and the active ones [7], [9]–[28]. The passive methods employ a resistor connected as a shunt for each cell to drain excess energy from the high-voltage cells [7]–[8]. Small size, low cost, and easy implementation are the outstanding advantages of this method. However, energy dissipation and heat problems are their critical disadvantages [7]. To overcome these drawbacks, active cell balancing circuits utilizing capacitors [9]–[18], inductors [19]–[21], or transformers [22]–[28] have been studied. Active balancing methods employ nondissipative energy-shuttling elements to move energy from strong cells to weak ones [7], [17], [18]. Among these active cell balancing methods, the switched-capacitor (SC)-based equalizers are promising due to the small size, ease of control, and ease of implementation [9]–[18], [29]–[30]. As shown in Fig. 1(a), for the classical SC equalizer, one capacitor is employed to shift energy between two adjacent cells [9]. Fig. 1(b) and (c) shows the two operation states of the classical SC equalizer. By switching the capacitors back and forth, the equalizer brings the cell voltages to an almost equal value [9]. However, energy is only

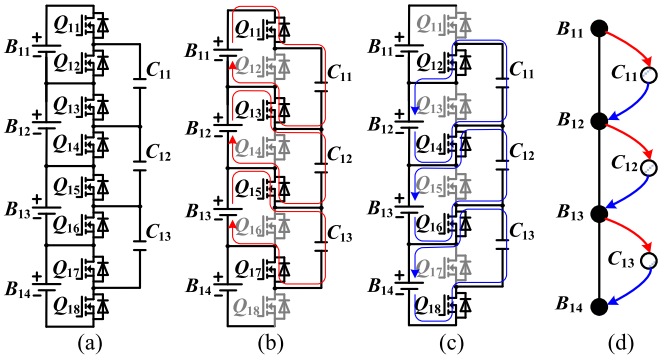

Fig. 1. Classical SC equalizer for four battery cells [9]. (a) Schematic diagram. (b) Operation state I. (c) Operation state II. (d) Balancing paths under the assumption of $V_{\mathrm{B}11} > V_{\mathrm{B}12} > V_{\mathrm{B}13} > V_{\mathrm{B}14}$.

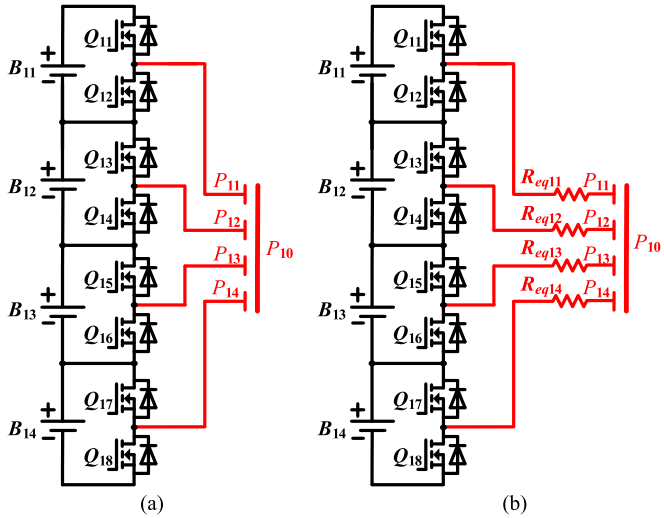

Fig. 2. Proposed SCCE for four cells connected in series. (a) Schematic diagram. (b) Equivalent circuit.

transferred from one cell to its adjacent cell through one capacitor during one switching cycle [9]. Fig. 1(d) shows the balancing paths under the assumption of $V_{B11} > V_{B12} > V_{B13} > V_{B14}$. Particularly, when the high-voltage cell and the low-voltage one are on the opposite ends of the battery string, it will take a long time and many steps to balance the cell voltages. Moreover, the balancing energy would have to travel through all the cells and capacitors, resulting in a severe penalty on the balancing efficiency and balancing speed.

In order to reduce the switching loss, a resonant SC equalizer was proposed in [10]. Based on the classical SC, an inductor L_0 is added to form a resonant LC converter, which operates alternatively between the charging state and discharging state with zero-current switching (ZCS) to automatically balance the cell voltages. However, this method has the same critical disadvantages as the classical SC solution, i.e., low balancing speed and efficiency for a long battery string. To increase the balancing speed, a double-tiered SC equalizer and a chain-structure of SC balancing circuit were proposed in [11] and [12]. These methods can, to a certain extent, improve the balancing speed by using additional capacitors and MOSFET switches. However, the balancing speed is still slow and the efficiency is also low as the increase of the number of the battery cells connected in series. Particularly, the equalizers are difficult to be modularized [31]. In order to improve these weaknesses, [13] and [14] propose two series-parallel SC equalizers. The working principles are that the switched capacitors are first connected in parallel with battery cells, being charged by or discharged to the battery cells, and then, all the capacitors are controlled to be connected in parallel, by which charge can flow from the higher voltage capacitors to the lower voltage ones [13]–[14]. By operating these two states alternatively, energy can be transferred from the higher voltage battery cells to the lower ones directly. This means the balancing speed could be significantly higher than the conventional one for a long battery string. However, the main disadvantage is that the switch number is twice of the classical SC solution. Therefore, [15] proposes a series of SC cell balancing circuits. With the same number of switches as the classical one, the methods achieve a high balancing speed, which does not rely on both of the number of battery cells and initial mismatch distribution of cell voltages.

Based on these works, the objective of this paper is to introduce an automatic switched-coupling-capacitor equalizer (SCCE), which achieves the direct and simultaneous equalization between any two cells in the battery string. Only two switches and one capacitor are needed for each battery cell, resulting in a small size and low cost. All MOSFETs are controlled by one pair of complementary pulse width modulation (PWM) signals, and energy can be automatically and directly delivered from any cells with higher voltages to any cells with lower voltages without the need of cell monitoring circuits, thereby leading to a high balancing efficiency and speed independent of the number of battery cells and the initial cell voltages. Contrary to the conventional modularized equalizers using additional components for the equalization among modules, the proposed SCCE can achieve the global equalization by connecting the common nodes of the switched coupling capacitors (SCCs), resulting in smaller size, lower cost, and higher balancing efficiency. The control for this system is very simple and the balancing operation can be carried out regardless of the battery working state of charging, discharging, or rest.

II. Proposed Equalizer

In this paper, an automatic SCCE is proposed, which can realize the any-cells-to-any-cells equalization for a battery string, which is an improvement of the work in [15].

A. Configuration of the Proposed Equalizer

Fig. 2 shows the schematic diagram and the equivalent circuit of the proposed SCCE applied to a four-cell battery string. Each battery cell is connected in parallel with two series-connected MOSFETs. Five capacitor plates (four small plates and one big plate) are used to form a coupling capacitor to transfer energy among cells. Each small plate ($P_{11} - P_{14}$) is connected to

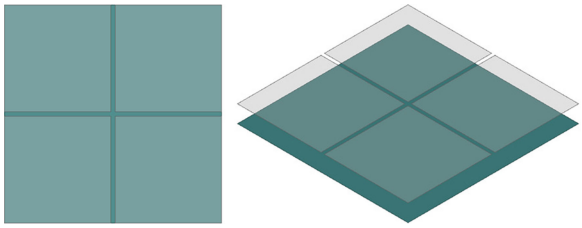

Fig. 3. The 3-D views of the proposed SCC for four cells.

the midpoint of the corresponding two series-connected MOSFETs. The big plate (P_{10}) is common to the four small plates, thus materializing the star connection. Fig. 3 shows the three-dimensional (3-D) views of the proposed SCC for four cells. In fact, the coupling capacitor can also be applied by four conventional capacitors connected in star.

The critical characteristics of the proposed SCCE are as follows:

1) Two MOSFET switches and one capacitor are needed for each cell, thereby leading to a small size and low cost.
2) Only one pair of complementary PWM signals are employed to control all MOSFET switches, by which automatic voltage equalization without the need of cell monitoring is achieved, showing a simple control.
3) Energy can be transferred automatically and directly from higher voltage cells at any position to lower voltage cells at any position, leading to a higher balancing efficiency and speed independent of the number of battery cells and the initial cell voltages.
4) Accurate voltage equalization is achieved without any requirements for the matching of the coupling capacitor and MOSFETs.
5) Contrary to the conventional modularized equalizers using additional components for the equalization among modules, the proposed method can achieve the equalization among modules by connecting the common nodes of the coupling capacitors, leading to smaller size, lower cost, and reduced loss related to the modularization.
6) The balancing operation can be carried out regardless of the battery working state of charging, discharging or rest.
7) The proposed SCCE can also be applied for other rechargeable batteries without any change or recalibration, such as nickel-cadmium batteries, lead-acid batteries, and nickel-metal-hydride batteries.

B. Operation Principles

The automatic any-cells-to-any-cells equalization among cells can be obtained by driving the MOSFET switches using one pair of complementary PWM signals, i.e., PWM+ and PWM–. The proposed equalizer has two steady working states in one switching period. Figs. 4 and 5 show the operating states and theoretical waveforms of the proposed equalizer, respectively. In order to simplify the analysis for the operation principles, it is assumed that the battery cell voltages follow $V_{B11} > V_{B12} > V_{B13} > V_{B14}$.

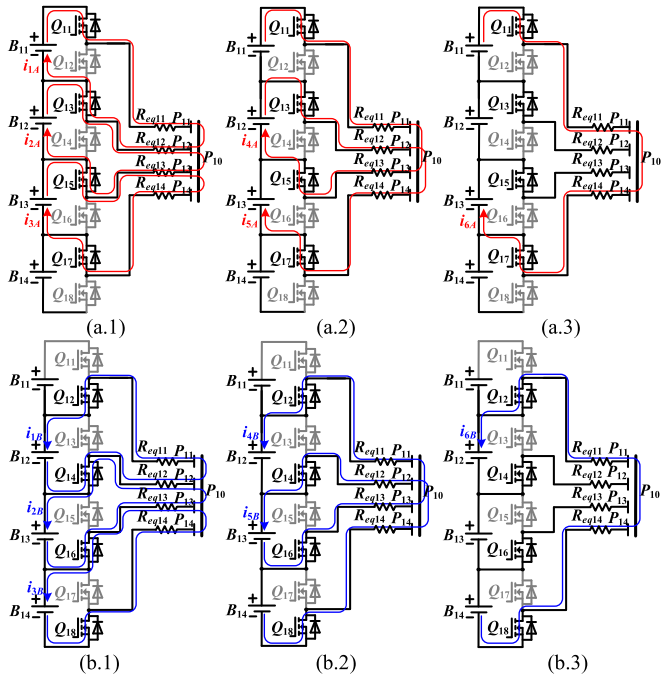

Fig. 4. Operating states of the proposed SCCE under the assumption of $V_{B11} > V_{B12} > V_{B13} > V_{B14}$. (a) State I. (b) State II.

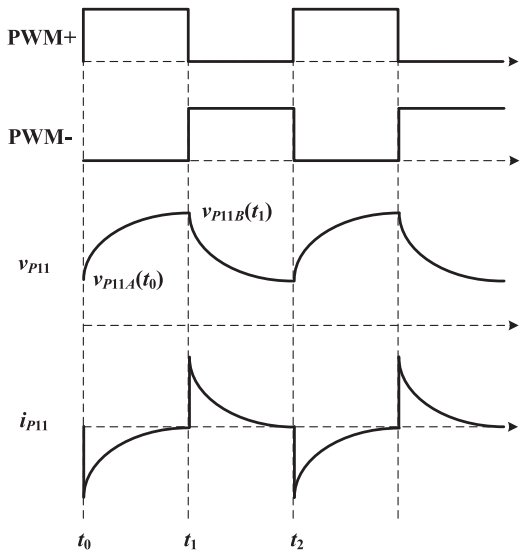

Fig. 5. Key waveforms of the proposed SCCE.

State I ($t_0 - t_1$): At t_0, mosfets Q_{11}, Q_{13}, Q_{15}, Q_{17} are turned on, and mosfets Q_{12}, Q_{14}, Q_{16}, Q_{18} are turned off. As shown in Fig. 4(a), the coupling capacitor is connected in parallel with the corresponding upper cells ($B_{11} - B_{13}$) through Q_{11}, Q_{13}, Q_{15}, and Q_{17}. As shown in Fig. 4(a.1)–(a.3), six discharging paths from battery cells are constructed.

As shown in Fig. 4(a.1), i_{1A} flows from B_{11} to $P_{11} - P_{10} - P_{12}$ through Q_{11} and Q_{13}. i_{2A} flows from B_{12} to $P_{12} - P_{10} - P_{13}$ through Q_{13} and Q_{15}. i_{3A} flows from B_{13} to $P_{13} - P_{10} - P_{14}$ through Q_{15} and Q_{17}. As shown in Fig. 4(a.2), i_{4A} flows from B_{11} and B_{12} to $P_{11} - P_{10} - P_{13}$ through Q_{11}

and Q_{15}. i_{5A} flows from B_{12} and B_{13} to $P_{12} - P_{10} - P_{14}$ through Q_{13} and Q_{17}. As shown in Fig. 4(a.3), i_{6A} flows from B_{11}, B_{12}, and B_{13} to $P_{11} - P_{10} - P_{14}$ through Q_{11} and Q_{17}. During this state, energy in the upper cells B_{11}-B_{13} is transferred to the coupling capacitor.

If the coupling capacitor and MOSFETs have identical characteristic, it is possible to assume the following:

$$C_{\rm eq} = C_{11} = C_{12} = C_{13} = C_{14} \tag{1}$$

$$R_{\rm eq} = R_{\rm eq11} = R_{\rm eq12} = R_{\rm eq13} = R_{\rm eq14} \tag{2}$$

where C_{1j}, $j = 1, 2, 3, 4$, represents the equivalent capacitance between the plates P_{1j} and P_{10}. $R_{\rm eq1}j$, $j = 1, 2, 3, 4$, represents the equivalent resistance in each branch. It is specified that the current flowing into a battery cell is positive, otherwise is negative.

During State I, the balancing currents across the capacitor plates can be expressed as

$$\begin{cases} i_{P11A} = i_{1A} + i_{4A} + i_{6A} \\ i_{P12A} = i_{2A} - i_{1A} + i_{5A} \\ i_{P13A} = i_{3A} - i_{2A} - i_{4A} \\ i_{P14A} = -i_{3A} - i_{5A} - i_{6A} \end{cases} \tag{3}$$

where i_{P1jA}, $j = 1, 2, 3, 4$, represents the balancing current across the plate P_{1j} during State I.

By using Kirchhoff's voltage law (KVL), the relationship between the cell voltages and the coupling capacitor voltages can be expressed as follows:

$$\begin{cases} \dfrac{V_{B11} - v_{P11A}(t_0) + v_{P12A}(t_0)}{s} \\ = \left(R_{\rm eq} + \dfrac{1}{s \cdot C_{\rm eq}}\right)(-i_{P11A} + i_{P12A}) \\ \dfrac{V_{B12} - v_{P12A}(t_0) + v_{P13A}(t_0)}{s} \\ = \left(R_{\rm eq} + \dfrac{1}{s \cdot C_{\rm eq}}\right)(-i_{P12A} + i_{P13A}) \\ \dfrac{V_{B13} - v_{P13A}(t_0) + v_{P14A}(t_0)}{s} \\ = \left(R_{\rm eq} + \dfrac{1}{s \cdot C_{\rm eq}}\right)(-i_{P13A} + i_{P14A}) \end{cases} \tag{4}$$

where $v_{P1jA}(t_0)$, $j = 1, 2, 3, 4$, represents the voltage between P_{1j} and P_{10} at t_0. V_{B1j}, $j = 1, 2, 3, 4$, is the cell voltage of B_{1j}.

By using Kirchhoff's current law (KCL), the relationship among the balancing currents across the coupling capacitor can be expressed as

$$i_{P11A} + i_{P12A} + i_{P13A} + i_{P14A} = 0. \tag{5}$$

By solving (4) and (5), the balancing currents across the coupling capacitor in the frequency domain can be obtained as

$$\begin{bmatrix} i_{P11A}(s) \\ i_{P12A}(s) \\ i_{P13A}(s) \\ i_{P14A}(s) \end{bmatrix} = \frac{1}{R_{\rm eq}} \cdot \frac{1}{s + \frac{1}{R_{\rm eq} \cdot C_{\rm eq}}} \cdot \mathbf{A} \cdot \mathbf{B} \tag{6}$$

where

$$\mathbf{A} = \begin{bmatrix} -\frac{3}{4} & -\frac{1}{2} & -\frac{1}{4} & \frac{1}{4} \\ \frac{1}{4} & -\frac{1}{2} & -\frac{1}{4} & \frac{1}{4} \\ \frac{1}{4} & \frac{1}{2} & -\frac{1}{4} & \frac{1}{4} \\ \frac{1}{4} & \frac{1}{2} & \frac{3}{4} & \frac{1}{4} \end{bmatrix}, \mathbf{B} = \begin{bmatrix} V_{B11} - v_{P11A}(t_0) + v_{P12A}(t_0) \\ V_{B12} - v_{P12A}(t_0) + v_{P13A}(t_0) \\ V_{B13} - v_{P13A}(t_0) + v_{P14A}(t_0) \\ 0 \end{bmatrix}. \tag{7}$$

By (6), the balancing currents can be turned into these in the time domain, given by

$$\begin{bmatrix} i_{P11A}(t) \\ i_{P12A}(t) \\ i_{P13A}(t) \\ i_{P14A}(t) \end{bmatrix} = \frac{1}{R_{\rm eq}} \cdot e^{-\frac{1}{R_{\rm eq} \cdot C_{\rm eq}}(t - t_0)} \cdot \mathbf{A} \cdot \mathbf{B} \tag{8}$$

where $t_0 < t < t_1$. Based on (8), Fig. 5 presents the theoretical waveform of the balancing current.

Using (6), the voltages across the coupling capacitor in the frequency domain can be derived as

$$\begin{bmatrix} v_{P11A}(s) \\ v_{P12A}(s) \\ v_{P13A}(s) \\ v_{P14A}(s) \end{bmatrix} = \frac{1}{s \cdot C_{\rm eq}} \begin{bmatrix} i_{P11A}(s) \\ i_{P12A}(s) \\ i_{P13A}(s) \\ i_{P14A}(s) \end{bmatrix} = \left(\frac{1}{s} - \frac{1}{s + \frac{1}{R_{\rm eq} \cdot C_{\rm eq}}}\right) \cdot \mathbf{A} \cdot \mathbf{B}. \tag{9}$$

Equation (9) can be turned into these in the time domain, shown as

$$\begin{bmatrix} v_{P11A}(t) \\ v_{P12A}(t) \\ v_{P13A}(t) \\ v_{P14A}(t) \end{bmatrix} = \left(1 - e^{-\frac{1}{R_{\rm eq} \cdot C_{\rm eq}}(t - t_0)}\right) \cdot \mathbf{A} \cdot \mathbf{B} + \begin{bmatrix} v_{P11A}(t_0) \\ v_{P12A}(t_0) \\ v_{P13A}(t_0) \\ v_{P14A}(t_0) \end{bmatrix} \tag{10}$$

where $t_0 < t < t_1$. According to (10), Fig. 5 presents the theoretical waveform of the coupling capacitor voltage.

At t_1, the balancing current drops to 0. Based on KVL, the relationship among the cell voltages and the coupling capacitor voltages can be expressed as

$$\begin{cases} v_{P11A}(t_1) - v_{P12A}(t_1) = V_{B11} \\ v_{P12A}(t_1) - v_{P13A}(t_1) = V_{B12} \\ v_{P13A}(t_1) - v_{P14A}(t_1) = V_{B13} \\ v_{P11A}(t_1) - v_{P13A}(t_1) = V_{B11} + V_{B12} \\ v_{P12A}(t_1) - v_{P14A}(t_1) = V_{B12} + V_{B13} \\ v_{P11A}(t_1) - v_{P14A}(t_1) = V_{B11} + V_{B12} + V_{B13}. \end{cases} \tag{11}$$

Equation (11) can be simplified as

$$\begin{cases} v_{P11A}(t_1) - v_{P12A}(t_1) = V_{B11} \\ v_{P12A}(t_1) - v_{P13A}(t_1) = V_{B12} \\ v_{P13A}(t_1) - v_{P14A}(t_1) = V_{B13}. \end{cases} \tag{12}$$

State II ($t_1 - t_2$): At t_1, MOSFETS Q_{12}, Q_{14}, Q_{16}, Q_{18} are turned ON, and MOSFETS Q_{11}, Q_{13}, Q_{15}, Q_{17} are turned OFF.

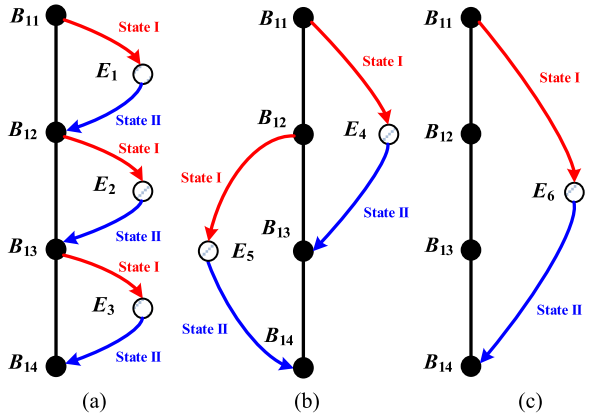

Fig. 6. Directed graphs of the proposed balancing methods under the assumption of $V_{B11} > V_{B12} > V_{B13} > V_{B14}$. (a) Balancing between adjacent two cells. (b) Balancing between every other cells. (c) Balancing between the first cell and last one. Note: E_1-E_6 represent the corresponding capacitor plates in the coupling capacitor as above.

As shown in Fig. 4(b), the coupling capacitor is connected in parallel with the corresponding lower cells ($B_{12} - B_{14}$) through Q_{12}, Q_{14}, Q_{16}, and Q_{18}. As shown in Fig. 4(b.1)-(b.3), six charging paths to battery cells are constructed.

As shown in Fig. 4(b.1), i_{1B} flows from $P_{11} - P_{10} - P_{12}$ to B_{12} through Q_{12} and Q_{14}, which achieves the energy transfer from B_{11} to B_{12}. i_{2B} flows from $P_{12} - P_{10} - P_{13}$ to B_{13} through Q_{14} and Q_{16}, which achieves the energy transfer from B_{12} to B_{13}. i_{3B} flows from $P_{13} - P_{10} - P_{14}$ to B_{14} through Q_{16} and Q_{18}, which achieves the energy transfer from B_{13} to B_{14}. Fig. 6(a) gives the directed graph of the energy transfer shown in Figs. 4(a.1) and (b.1), demonstrating that the proposed SCCE can achieve the conventional adjacent-cell-to-adjacent-cell equalization.

As shown in Fig. 4(b.2), i_{4B} flows from $P_{11} - P_{10} - P_{13}$ to B_{12} and B_{13} through Q_{12} and Q_{16}, which achieves the energy transfer from B_{11} to B_{13}. i_{5B} flows from $P_{12} - P_{10} - P_{14}$ to B_{13} and B_{14} through Q_{14} and Q_{18}, which achieves the energy transfer from B_{12} to B_{14}. Fig. 6(b) gives the directed graph of the energy transfer shown in Fig. 4(a.2) and (b.2), demonstrating that the proposed SCCE achieves the equalization between every other cells.

As shown in Fig. 4(b.3), i_{6B} flows from $P_{11} - P_{10} - P_{14}$ to B_{12}, B_{13}, and B_{14} through Q_{12} and Q_{18}, which achieves the energy transfer from B_{11} to B_{14}. Fig. 6(c) gives the directed graph of the energy transfer shown in Fig. 4(a.3) and (b.3), proving that the proposed SCCE achieves the direct equalization between the first cell and last one in a battery string.

It can be seen that the proposed equalizer can transfer energy directly between any two cells in a battery string.

During State II, the balancing current across the capacitor plates can be expressed as

$$\begin{cases} i_{P11B} = i_{1B} + i_{4B} + i_{6B} \\ i_{P12B} = -i_{1B} + i_{2B} + i_{5B} \\ i_{P13B} = -i_{2B} + i_{3B} - i_{4B} \\ i_{P14B} = -i_{3B} - i_{5B} - i_{6B} \end{cases} \tag{13}$$

where i_{P1jB}, $j = 1, 2, 3, 4$, represents the balancing current across P_{1j} during State II.

By using KVL, the relationship among the cell voltages and the coupling capacitor voltages can be expressed as

$$\begin{cases} \dfrac{v_{P11B}(t_1) - V_{B12} - v_{P12B}(t_1)}{s} \\ = \left(R_{eq} + \dfrac{1}{s \cdot C_{eq}}\right)(i_{P11B} - i_{P12B}) \\ \dfrac{v_{P12B}(t_1) - V_{B13} - v_{P13B}(t_1)}{s} \\ = \left(R_{eq} + \dfrac{1}{s \cdot C_{eq}}\right)(i_{P12B} - i_{P13B}) \\ \dfrac{v_{P13B}(t_1) - V_{B14} - v_{P14B}(t_1)}{s} \\ = \left(R_{eq} + \dfrac{1}{s \cdot C_{eq}}\right)(i_{P13B} - i_{P14B}) \end{cases} \tag{14}$$

where $v_{P1jB}(t_1)$, $j = 1, 2, 3, 4$, represents the voltage between P_{1j} and P_{10} at t_1.

By using KCL, the relationship among the balancing currents across the coupling capacitor can be expressed as

$$i_{P11B} + i_{P12B} + i_{P13B} + i_{P14B} = 0. \tag{15}$$

By solving (14) and (15), the balancing currents in the frequency domain can be obtained as

$$\begin{bmatrix} i_{P11B}(s) \\ i_{P12B}(s) \\ i_{P13B}(s) \\ i_{P14B}(s) \end{bmatrix} = \frac{1}{R_{eq}} \cdot \frac{1}{s + \frac{1}{R_{eq} \cdot C_{eq}}} \cdot \mathbf{C} \cdot \mathbf{D} \tag{16}$$

where

$$\mathbf{C} = \begin{bmatrix} \frac{3}{4} & \frac{1}{2} & \frac{1}{4} & \frac{1}{4} \\ -\frac{1}{4} & \frac{1}{2} & \frac{1}{4} & \frac{1}{4} \\ -\frac{1}{4} & -\frac{1}{2} & \frac{1}{4} & \frac{1}{4} \\ -\frac{1}{4} & -\frac{1}{2} & -\frac{3}{4} & \frac{1}{4} \end{bmatrix}, \mathbf{D} = \begin{bmatrix} v_{P11B}(t_1) - V_{B12} - v_{P12B}(t_1) \\ v_{P12B}(t_1) - V_{B13} - v_{P13B}(t_1) \\ v_{P13B}(t_1) - V_{B14} - v_{P14B}(t_1) \\ 0 \end{bmatrix}. \tag{17}$$

By (16), the balancing currents can be transferred into these in the time domain, given by

$$\begin{bmatrix} i_{P11B}(t) \\ i_{P12B}(t) \\ i_{P13B}(t) \\ i_{P14B}(t) \end{bmatrix} = \frac{1}{R_{eq}} \cdot e^{-\frac{1}{R_{eq} \cdot C_{eq}}(t - t_1)} \cdot \mathbf{C} \cdot \mathbf{D} \tag{18}$$

where $t_1 < t < t_2$. Using (16), the voltages across the coupling capacitor in the frequency domain can be achieved as

$$\begin{bmatrix} v_{P11B}(s) \\ v_{P12B}(s) \\ v_{P13B}(s) \\ v_{P14B}(s) \end{bmatrix} = \left(\frac{1}{s} - \frac{1}{s + \frac{1}{R_{eq} \cdot C_{eq}}}\right) \cdot \mathbf{C} \cdot \mathbf{D} \tag{19}$$

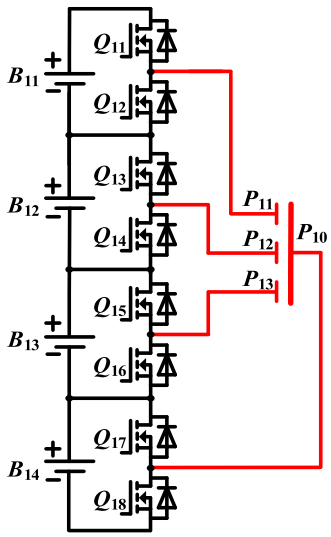

Fig. 7. Simplified SCCE for four cells connected in series.

Equation (19) can be turned into these in the time domain, shown as

$$\begin{bmatrix} v_{P11B}(t) \\ v_{P12B}(t) \\ v_{P13B}(t) \\ v_{P14B}(t) \end{bmatrix} = \left(1 - e^{-\frac{1}{Req \cdot Ceq}(t-t_1)}\right) \cdot \mathbf{C} \cdot \mathbf{D} + \begin{bmatrix} v_{P11B}(t_1) \\ v_{P12B}(t_1) \\ v_{P13B}(t_1) \\ v_{P14B}(t_1) \end{bmatrix} \tag{20}$$

where $t_1 < t < t_2$.

At t_2, the balancing current drops to 0. Based on KVL, the relationship among the cell voltages and the coupling capacitor voltages can be expressed as

$$\begin{cases} v_{P11B}(t_2) - v_{P12B}(t_2) = V_{B12} \\ v_{P12B}(t_2) - v_{P13B}(t_2) = V_{B13} \\ v_{P13B}(t_2) - v_{P14B}(t_2) = V_{B14} \\ v_{P11B}(t_2) - v_{P13B}(t_2) = V_{B12} + V_{B13} \\ v_{P12B}(t_2) - v_{P14B}(t_2) = V_{B13} + V_{B14} \\ v_{P11B}(t_2) - v_{P14B}(t_2) = V_{B12} + V_{B13} + V_{B14}. \end{cases} \tag{21}$$

Equation (21) can be simplified as

$$\begin{cases} v_{P11B}(t_2) - v_{P12B}(t_2) = V_{B12} \\ v_{P12B}(t_2) - v_{P13B}(t_2) = V_{B13} \\ v_{P13B}(t_2) - v_{P14B}(t_2) = V_{B14}. \end{cases} \tag{22}$$

It is important to note that the solutions for (12) and (22) are not unique, indicating the uncertainty of the capacitor voltages and the floating potential of P_{10}. This is because there are more capacitors than needed. In another word, one capacitor can be removed from the switched-coupling capacitor, and the simplified topology is shown in Fig. 7. In fact, the redundant capacitor only affects the balancing currents, not the final cell voltages. This simplified equalization circuit has the same operation principles as the structure shown in Fig. 2, thereby not described in detail here.

TABLE I
BALANCING PATHS BETWEEN ANY TWO CELLS

Paths across the SCC	B_{11}	B_{12}	B_{13}	B_{14}
B_{11}	–	P_{11}-P_{10}-P_{12}	P_{11}-P_{10}-P_{13}	P_{11}-P_{10}-P_{14}
B_{12}	P_{11}-P_{10}-P_{12}	–	P_{12}-P_{10}-P_{13}	P_{12}-P_{10}-P_{14}
B_{13}	P_{11}-P_{10}-P_{13}	P_{12}-P_{10}-P_{13}	–	P_{13}-P_{10}-P_{14}
B_{14}	P_{11}-P_{10}-P_{14}	P_{12}-P_{10}-P_{14}	P_{13}-P_{10}-P_{14}	–

Table I summarizes the balancing paths between any two cells. It can be seen that due to the proposed coupling capacitor, energy can be directly transferred from higher voltage cells at any position to lower voltage cells at any position, leading to a high balancing efficiency and speed.

C. Equalizing Power and Efficiency

The balancing power of each cell can be calculated as

$$P_{B1j} = V_{B1j} \cdot I_{B1j} \tag{23}$$

where $j = 1, 2, 3, 4$. V_{B1j} is the cell voltage of the battery cell B_{1j}. I_{B1j} is the RMS balancing current flowing out of or into B_{1j}, which can be expressed as

$$I_{B1j} = \sqrt{\frac{1}{T}\int_0^{\frac{T}{2}} [i_{B1j}(t)]^2 dt} \text{ or } I_{B1j} = \sqrt{\frac{1}{T}\int_{\frac{T}{2}}^{T} [i_{B1j}(t)]^2 dt} \tag{24}$$

where T is the switching period. $i_{B1j}(t)$ is the AC balancing current flowing out of or into B_{1j}.

The balancing efficiency is obtained as

$$\eta_e = \frac{\sum_{j=1}^{4} IF(P_{B1j} > 0)}{\left|\sum_{j=1}^{4} IF(P_{B1j} < 0)\right|} \times 100\% \tag{25}$$

where

$$\begin{cases} IF(P_{B1j} < 0) = \begin{cases} P_{B1j}, & \text{when } P_{B1j} < 0 \\ 0, & \text{when } P_{B1j} \geq 0 \end{cases} \\ IF(P_{B1j} > 0) = \begin{cases} P_{B1j}, & \text{when } P_{B1j} > 0 \\ 0, & \text{when } P_{B1j} \leq 0 \end{cases} \end{cases} . \tag{26}$$

It can be seen that the balancing efficiency is determined by the cell charge power and the cell discharge power.

D. Modularization of the Proposed SCCE

As shown in Fig. 8, a modularization concept of the proposed SCCE is applied to an eight-cell series-connected battery string, which is divided into two separate four-cell modules. It can be seen that the global equalization among cells is achieved through the connection of the common nodes of the two coupling capacitors CC_1 and CC_2. Contrary to the conventional modularized equalizers using additional components for the equalization among modules, the proposed modularization method shares a single equalizer for the equalization among cells and modules, leading to smaller size, lower cost, and reduced loss with respect to the modularization.

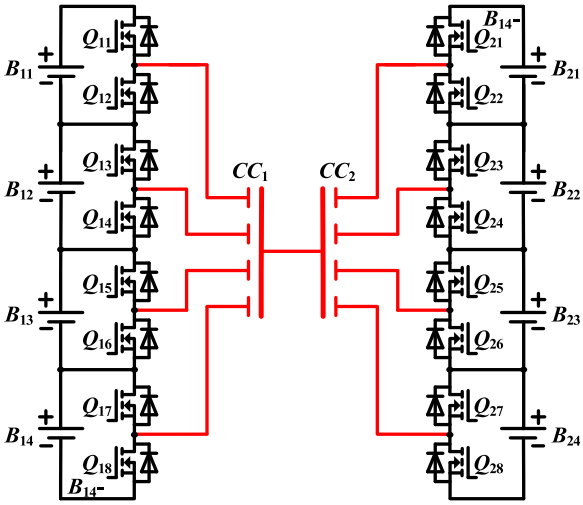

Fig. 8. Modularized structure of the proposed SCCE for an eight-cell battery string, which is divided into two separate modules.

E. Comparison With Conventional Battery Equalizers

As shown in Figs. 1 and 2, the proposed SCCE has the same number of MOSFETs as the conventional topology, and needs n capacitors compared with the conventional method with the requirement of $n-1$ capacitors. Thus, it can be concluded that the MOSFET and capacitor numbers of the presented solution are comparable to the existing SC method. Moreover, all switches employed in the two methods withstand the same voltage stress.

For the classical SC topology, the maximum voltage stress of capacitors is the cell voltage, i.e., V_B. The capacitance of each capacitor is $C_{\rm eq}$, which is in the range of 20 – 1000 μF [9]. The proposed coupling capacitor can be applied by four capacitors connected in star, as shown in Fig. 2. In each balancing path, there are two capacitors connected in series. Therefore, the capacitance of each capacitor is required to be $2C_{\rm eq}$ to achieve the same balancing capacitance as the classical SC topology. As shown in Fig. 4, during each operating state, the first and last capacitors of the coupling capacitor are connected in parallel with n-1 cells. Thus, the voltage stress for these two capacitors is $(n-1)\cdot V_B/2$. n is the number of cells connected in series in the battery string. It can be observed that the voltage stress and capacitance of capacitors in the proposed equalizer are higher and larger than the classical solution. Nonetheless, the cost of the balancing circuits depends mainly on the MOSFETs, gate drivers, isolated power supplies, and the controllers. The capacitors only accounts for a fraction of the cost of the balancing circuits. Thus, the implementation cost of the proposed method is slightly higher than that of the conventional approach. The extra cost is due to the required higher breakdown voltage and twice capacitance of capacitors. However, the number of the switches and the control complexity remain the same.

If the source cell is separated from the target cell by several other cells, it takes several balancing steps for the classical SC method to transfer charge between the two cells. Shang *et al.* [17] gives the average balancing step to complete the charge transportation as follows:

$$Step_{\rm avg}=\frac{\frac{n(n-1)(n+1)}{3}}{n^2-n}=\frac{n+1}{3} \tag{27}$$

where n is the number of cells connected in series in the battery string. Equation (27) shows the balancing speed will decline along with the increase of the number of battery cells.

Consequently, the average balancing efficiency of the classical SC method is obtained by

$$\eta_{avg}=\eta_e^{\frac{n+1}{3}} \tag{28}$$

where η_e is the balancing efficiency between adjacent two cells. Equation (28) shows the average balancing efficiency is enormously attenuated by the one-by-one energy transfer path in spite of the higher balancing efficiency between adjacent two cells.

For the proposed solution, energy can be transferred directly from higher voltage cells at any position to lower voltage cells at any position. Theoretically, it only takes one balancing step for the proposed solution to complete the charge transportation from the source cell to the target one without intermediate steps. Therefore, the balancing efficiency and speed of the proposed method are independent of the number of battery cells and the initial cell voltages.

According to the above analysis, Table II gives the comparison of the proposed equalizer with the classical SC solution in terms of the cost, balancing speed, and efficiency.

In order to evaluate the proposed topology quantitatively and systematically, Table III illustrates the comparison of the proposed equalizer with conventional ones under the assumption of a series-connected battery string consisting of n cells. The comparison focuses on the components used in equalizers and the balancing performances. "Components" consists of the numbers of switches (SW), resistors (R), inductors (L), capacitors (C), diodes (D), and transformers (T). Twelve parameters are employed to evaluate the balancing performances. Each parameter is fuzzified into five fuzzy scales, for which "1", "2", "3", "4", and "5" represent the worst, bad, neutral, good, and best performances, respectively. The balancing performance parameters are cost (S_1), efficiency (S_2), automatic balancing capability (S_3), bidirectional balancing capability (S_4), energy flow (1: adjacent cell to cell, 5: any cells to any cells) (S_5), speed (S_6), implementation possibility (S_7), complexity (S_8), size (S_9), modularization (S_{10}), switch voltage stress (S_{11}), and switch current stress (S_{12}). By applying a large weight (i.e., 1.5) to cost and efficiency, and a small weight (i.e., 1) to the other parameters, an average score $S_{\rm avg}$ is obtained in the last column of Table III, by which a quantitative comparison can be intuitively carried out. It can be observed that the proposed equalizer has the highest average score, and has the advantages of low cost, low size, high efficiency, high speed, low voltage stress, and easy modularization, making the proposed topology suitable to be applied to a long series-connected battery string. However, it is important to note that the parameter weights should be modified according to the practical application, which is helpful to select a suitable balancing topology depending on different applications.

TABLE II
COMPARISON OF THE PROPOSED EQUALIZER WITH THE CLASSICAL SC SOLUTION IN TERMS OF THE COST, BALANCING SPEED, AND EFFICIENCY

Equalizers	Number of MOSFETs	Number of capacitors	Breakdown voltage of capacitors	Capacitance of capacitors capacitors	Cost	Balancing speed ($Step_{avg}$)	Balancing efficiency
The classic SC	$2n$	$n-1$	V_B	C_{eq}	Low	$\frac{n+1}{3}$	$\eta_e \frac{n+1}{3}$
The proposed SCCE	$2n$	n	$\frac{(n-1)\cdot V_B}{2}$	$2C_{eq}$	Slightly high	1	η_e

TABLE III
QUANTITATIVE AND SYSTEMATIC COMPARISON OF THE PROPOSED BATTERY EQUALIZER WITH THE CONVENTIONAL ONES

Balancing performances	Components						S_1	S_2	S_3	S_4	S_5	S_6	S_7	S_8	S_9	S_{10}	S_{11}	S_{12}	S_{avg}
	SW	R	L	C	D	T													
Dissipative equalizer [8]	n	n	0	0	0	0	5	1	1	1	1	5	1	5	5	3	5	1	2.85
SC [9]	$2n$	0	0	$n-1$	0	0	5	3	5	5	1	2	4	5	5	3	5	4	3.92
ZCS SC [10]	$2n$	0	$n-1$	$n-1$	0	0	3	3	5	5	1	2	3	4	3	3	5	5	3.46
Double-tiered SC[11]	$2n$	0	0	n	0	0	4	3	5	5	2	2	3	4	4	3	5	4	3.65
Chain structure of SC [12]	$2n+4$	0	0	$n+1$	0	0	4	4	5	5	2	3	3	4	4	2	5	4	3.77
Series-parallel SC [13]	$4n$	0	0	n	0	0	3	4	5	5	5	5	3	4	3	3	2	4	3.81
Automatic SC [14]	$4n-3$	0	0	n	0	0	3	4	5	5	5	5	3	4	3	3	2	4	3.81
Direct ZCS SC [16]	$2n+10$	0	1	1	0	0	3	4	2	5	2	2	3	2	3	2	1	5	2.88
Wave trap [22]	2	0	n	n	n	n	2	3	1	1	3	3	1	1	2	1	1	5	2.04
Forward conversion [25]	n	0	0	n	0	1	3	5	5	5	5	5	5	3	4	5	4	5	4.46
Flyback conversion [26]	$2n-2$	0	0	0	$2n-2$	1	3	4	2	1	3	3	2	2	3	3	2	2	2.58
Proposed equalizer	$2n$	0	0	n	0	0	4	4	5	5	5	5	5	5	5	5	5	4	4.69

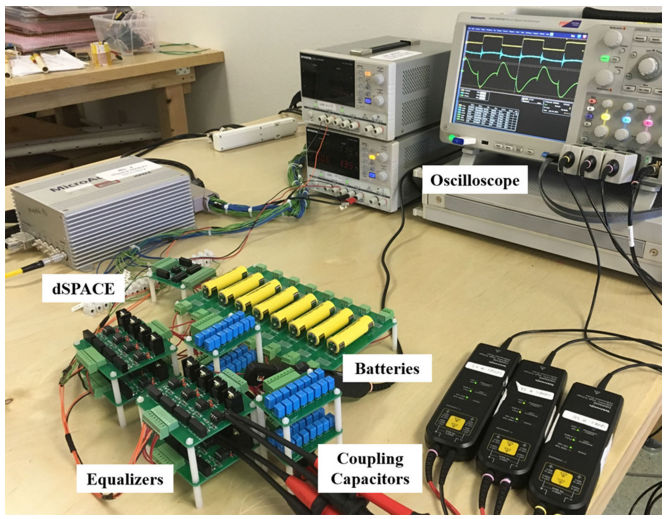

Fig. 9. Photograph of the implemented prototype for the SCCE.

III. EXPERIMENTAL RESULTS

Fig. 9 shows the implemented prototype for eight 1100-mAh $LiFePO_4$ cells connected in series. STP220N6F7 MOSFETs with 2.4-mΩ drain-source on-resistance were used for switches $Q_{11} - Q_{18}$. dSPACE was used for the digital control. The coupling capacitor was applied by the conventional single capacitors connected in star. The preferred selection principles of capacitors are summarized as follows:

1) Nonare selected to achieve the bidirectional energy transfer.
2) The breakdown voltage of capacitors should be higher than $(n-1)\cdot V_B/2$.
3) The appropriate capacitances of capacitors will be in the range of 20 –1000 μF [9]. In this paper, the capacitance is 28.3 μF, and the equivalent resistance is 67 mΩ.
4) The capacitance tolerance of capacitors is allowed. The consistency of the capacitances only affects the balancing currents, not the final balanced voltage of the battery string. In another word, precise equalization can be performed without any requirement for the capacitance matching or tight tolerances.

Fig. 10 shows the experimental waveforms of the balancing current i_{P11} and the capacitor voltage v_{P11}. A switching frequency that is too low or too high would bring the balancing efficiency and speed drop because of the rise in the equivalent resistance [15]. In order to achieve a higher balancing efficiency and speed, the coupling capacitor should be fully charged and fully discharged per switching cycle. The switching frequency can be selected properly by the balancing current waveform. Therefore, the proposed prototype is recommended to operate at about 28.58 kHz to ensure that the MOSFETs are switched at the near zero-current state. As shown in Fig. 10, when MOSFETs $Q_{11}, Q_{13}, Q_{15}, Q_{17}$ are turned ON, the balancing current i_{P11} flows from the upper cells to the SCC. The SCC is charged by the upper cells. So, the voltage across the SCC begins to increase. When MOSFETs $Q_{12}, Q_{14}, Q_{16}, Q_{18}$ are turned ON, i_{P11} flows from the SCC to the corresponding lower cells. The lower cells are charged by the SCC, so the voltage across the SCC begins to decrease. The RMS balancing current is approximately 0.97 A. Compared with the theoretical waveforms shown in Fig. 5, we can observe that the changes in the balancing current are resisted, to some extent, by the stray inductances in circuits, which also causes the voltage spikes in

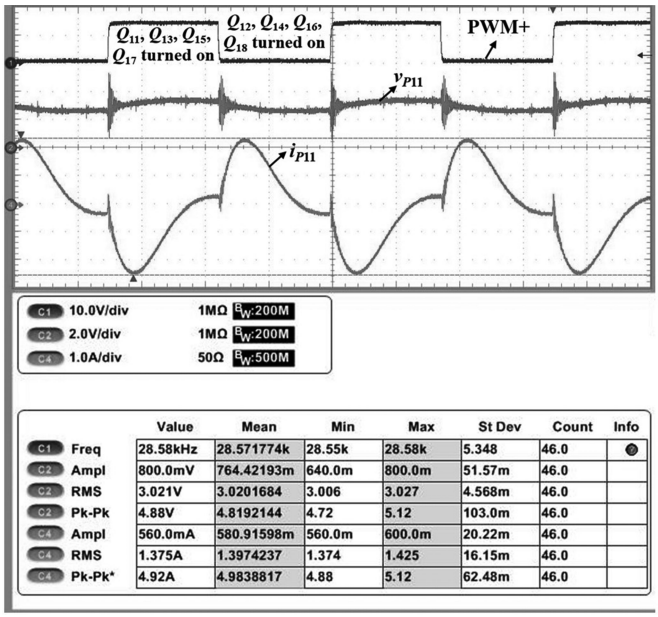

Fig. 10. Experimental waveforms of the proposed SCCE.

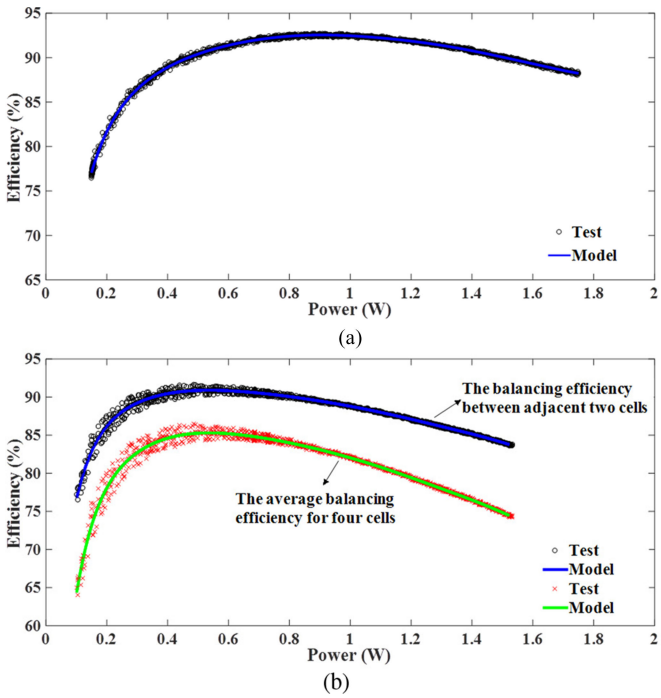

Fig. 11. Measured balancing efficiency η_e as a function of the output power at the frequency of $f = 28.58$ kHz. (a) Proposed method for four cells. (b) Classical SC method.

the capacitor voltage during the turn-ON and turn-OFF transitions of the MOSFETs. Overall, the experimental waveforms agree with the theoretical waveforms shown in Fig. 5.

Based on (25), Fig. 11(a) shows the measured efficiency η_e as a function of the output power at the frequency of $f = 28.58$ kHz. When the output power increases from 0.15 W to 0.875 W, η_e increases from 76.5% to 92.7%. When the output power increases from 0.875 to 1.75 W, η_e decreases from 92.7% to 88.2%. The measured peak efficiency is 92.7% at the output power of 0.875 W. Moreover, the measured efficiency is independent of the number of battery cells and the initial cell voltages. These results show that the proposed equalizer can work with a high efficiency over a wide range of loading conditions. In order to prove the improvement of the balancing efficiency of the proposed structure, Fig. 11(b) shows the balancing efficiencies of the classical SC equalizer. It can be observed that the balancing efficiency between adjacent two cells is comparable to the proposed SCCE. However, according to (28), the average balancing efficiency is lower than the proposed SCCE. Moreover, the average efficiency of the classical SC method will decline along with the increase of the number of battery cells.

Fig. 12 shows the equalization results for four $LiFePO_4$ cells with different cell permutations at $f = 28.58$ kHz. The initial cell voltages are 3.209, 3.160, 3.110, and 2.679 V, respectively. The maximum initial voltage gap among cells is 0.53 V. From Fig. 12(a)–(j), it can be observed that under any cell permutation, the equalization for cells can be well executed by the proposed SCCE. Table IV illustrates the balancing time, balanced voltage, and voltage gap among cells after balancing. These results prove that the proposed balancing operation is independent of the cell positions in the series-connected battery string, demonstrating the strong robustness of the proposed equalizer.

In order to further verify the validity of the proposed equalizer, Fig. 13 shows the equalization results with different initial voltages. We can observe that the proposed equalizer can gather simultaneously the cell voltages together under any imbalance situation of the series-connected string, showing the good performance of the proposed equalizer. Table V summarizes the balancing performances with different initial voltages.

In order to show the advantages of the proposed equalizer over the conventional equalizers, Fig. 14 shows the balancing results of the classical SC method. The initial cell voltages are the same as shown in Fig. 13. It can be observed that due to the adjacent-cell-to-cell equalization, some cell voltages first go down and then go up, which leads to the unnecessary energy loss. Table VI summarizes the balancing time, balanced voltage, and voltage gap among cells after balancing. Comparing the balancing results shown in Table VI with these in Table V, it can be concluded that the proposed method have advantages over the conventional one in the balancing speed, efficiency, and equalization performance.

To verify the validity of the proposed simplified equalizer shown in Fig. 7 and Fig. 15 shows the equalization result with the same initial voltages as Fig. 12(a). It can be observed that the cell equalization is also well executed by the simplified equalizer. However, the balancing speed for B_{14} is significantly improved due to the absence of P_{14} for the coupling capacitor. In fact, for the simplified equalizer, capacitance C_{14} can be deemed to be infinite. Therefore, this also proves that the consistency of the capacitances only affects the balancing currents, not the final balanced voltages of the battery string.

Fig. 16 shows the modularized equalization results for eight $LiFePO_4$ cells, which are divided into two separate four-cell modules at $f = 28.58$ kHz. As shown in Fig. 16(a), the initial cell

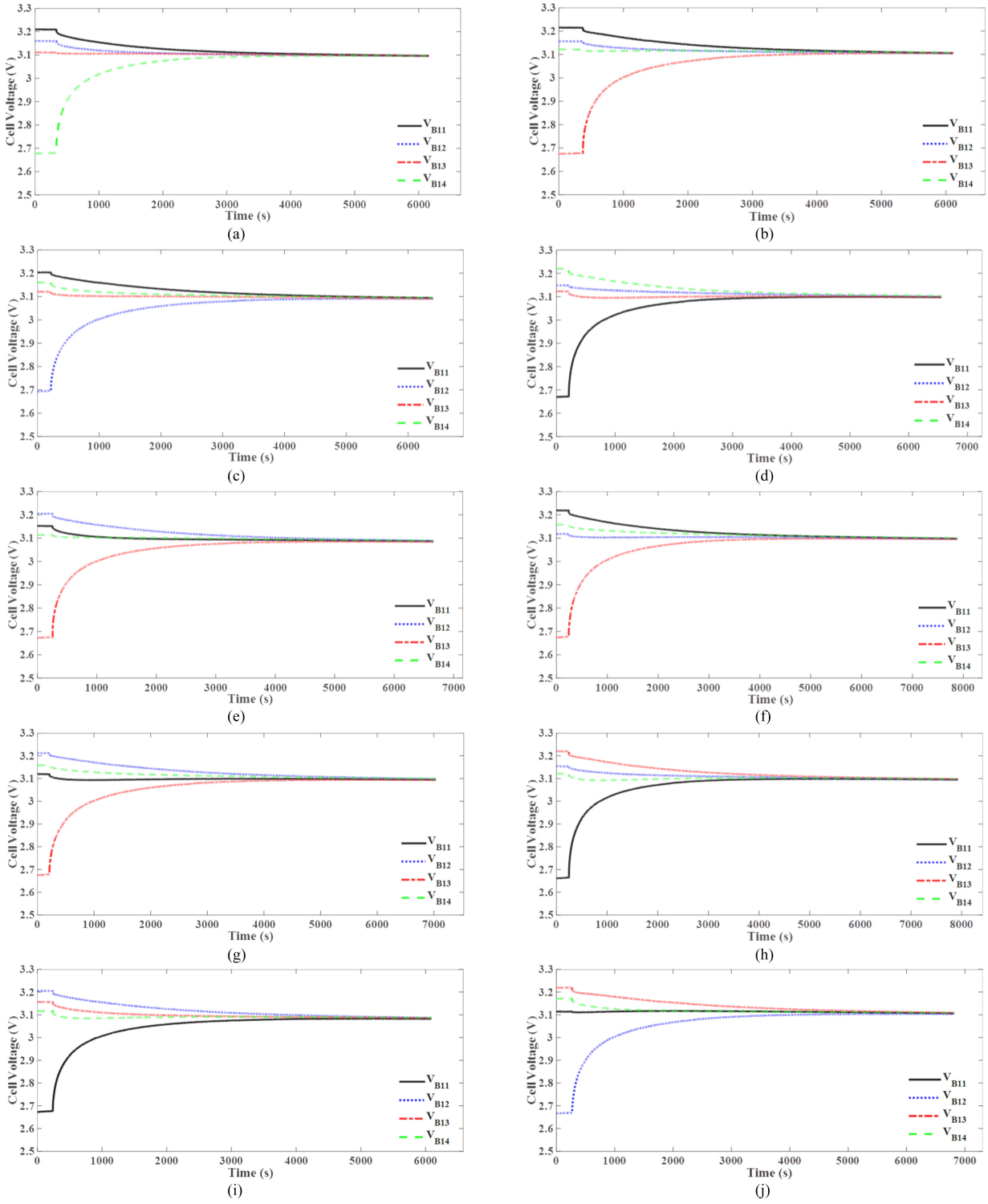

Fig. 12. Experimental results of the proposed equalizer for four $LiFePO_4$ cells with different cell permutations at $f = 28.58$ kHz.

TABLE IV
BALANCING RESULTS OF THE PROPOSED METHOD WITH DIFFERENT CELL PERMUTATIONS

Fig. 12	(a)	(b)	(c)	(d)	(e)	(f)	(g)	(h)	(i)	(j)
Balancing time (s)	6000	6000	6000	6000	6000	7000	7000	7000	6000	6800
Balanced voltage (V)	3.096	3.106	3.093	3.101	3.089	3.099	3.097	3.099	3.086	3.107
Voltage gap after balancing (mV)	2	3	4	6	6	6	6	4	5	6

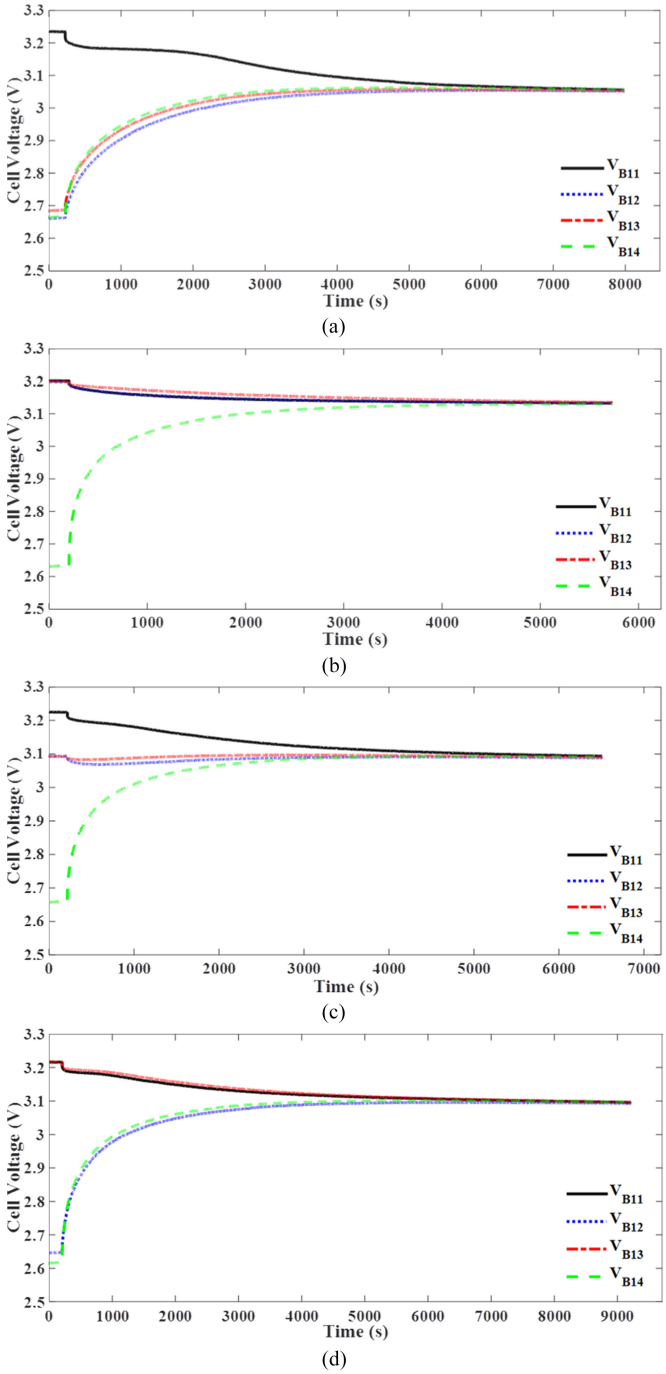

Fig. 13. Experimental results of the proposed equalizer for four $LiFePO_4$ cells with different initial voltages at $f = 28.58$ kHz.

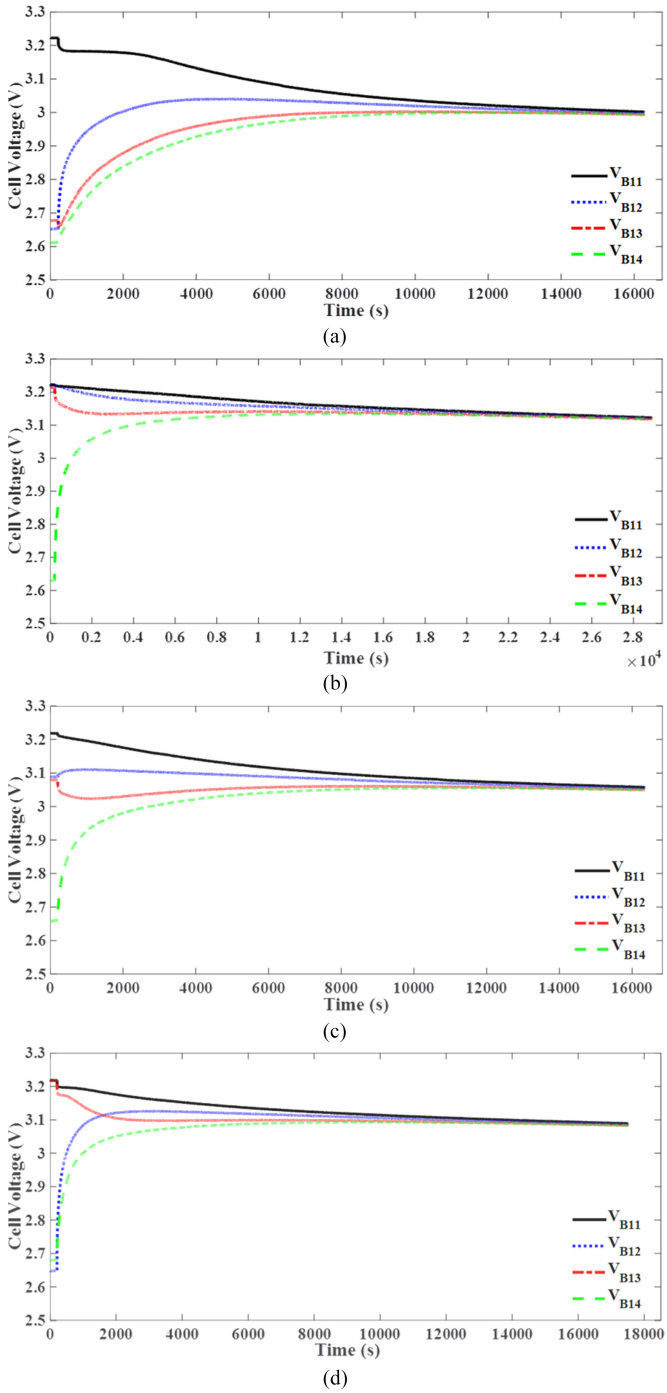

Fig. 14. Experimental results of the classical SC method for four $LiFePO_4$ cells with different initial voltages at $f = 28.58$ kHz.

TABLE V
BALANCING RESULTS OF THE PROPOSED METHOD WITH DIFFERENT INITIAL VOLTAGES

Fig. 13	(a)	(b)	(c)	(d)
Balancing time (s)	7945	5727	6940	9209
Balanced voltage (V)	3.055	3.133	3.084	3.096
Voltage gap after balancing (mV)	5	5	6	4

TABLE VI
BALANCING RESULTS OF THE CLASSICAL SC METHOD WITH DIFFERENT INITIAL VOLTAGES

Fig. 14	(a)	(b)	(c)	(d)
Balancing time (s)	16270	28880	16340	17500
Balanced voltage (V)	2.997	3.119	3.052	3.085
Voltage gap after balancing (mV)	8	4	9	5

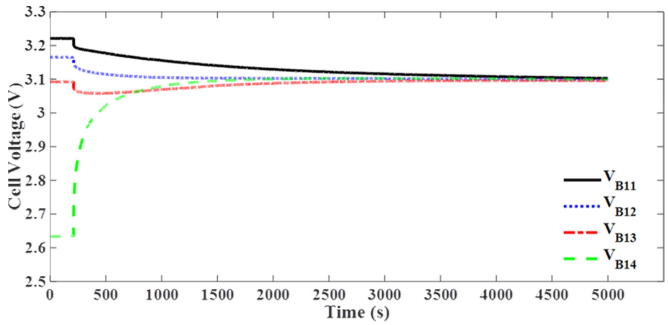

Fig. 15. Experimental result of the simplified equalizer for four $LiFePO_4$ cells at $f = 28.58$ kHz.

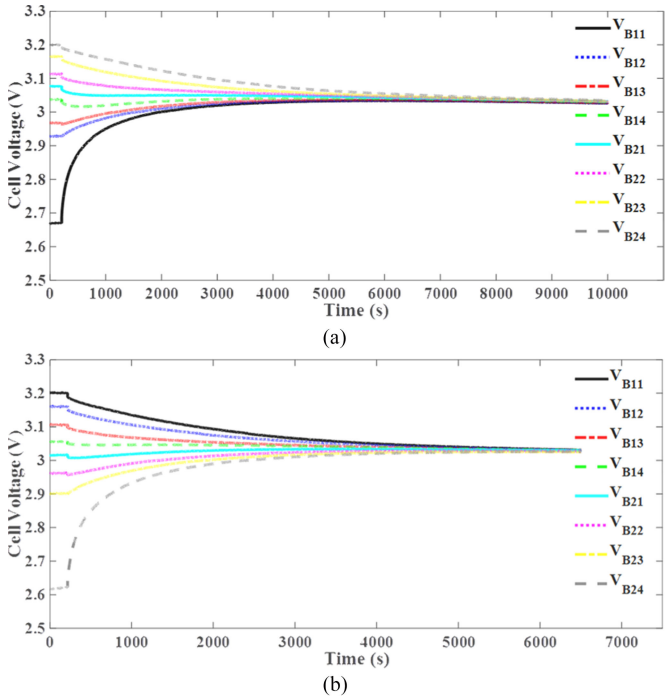

Fig. 16. Modularized equalization results for eight $LiFePO_4$ cells, which are divided into two four-cell modules at $f = 28.58$ kHz.

voltages are 2.669, 2.928, 2.968, 3.038, 3.077, 3.114, 3.165, and 3.200 V, respectively. The initial maximum voltage gap among cells is 0.531 V. After about 10000 s, a balanced voltage of 3.030 V is achieved, and the voltage gap among cells is 9 mV. Fig. 16(b) shows the equalization result with different initial voltages. The initial cell voltages are 3.202, 3.161, 3.107, 3.057, 3.016, 2.963, 2.901, and 2.620 V, respectively. The cell voltages are balanced after about 6500 s with the balanced voltage of 3.029 V and the voltage gap of 6 mV. These experimental results verify the validity of the proposed modularized equalizer.

IV. Conclusion

An automatic any-cells-to-any-cells equalizer based on switched coupling capacitor is proposed and a prototype for four cells is implemented. The configuration of the proposed equalizer, the operation principles, the modular design, the comparison with the conventional SC equalizers, and the cell balancing performance are presented in this paper. Experimental results demonstrate that the proposed circuit has outstanding any-cells-to-any-cells equalization performance with a simple control, and the energy transfer efficiency among cells can reach up to 92.7%. The proposed equalizer achieves the automatic voltage equalization without cell voltage monitoring, obtains the global equalization for a battery string without the requirement of additional equalizers for modules, and has lower voltage stress on MOSFETs, which ensures the system high reliability and ease of implementation. In the future, inductors will be considered to be added in the proposed topology to achieve soft switching and restrain the large rush current because of the zero initial voltages of capacitors at the beginning of balancing.

References

[1] L. Lu, X. Han, J. Li, J. Hua, and M. Ouyang, "A review on the key issues for lithium-ion battery management in electric vehicles," *J. Power Sources*, vol. 226, pp. 272–288, Mar. 2013.

[2] B. Xia, Y. Shang, T. Nguyen, and C. Mi, "A correlation based fault detection method for short circuits in battery packs," *J. Power Sources*, vol. 337, pp. 1–10, Jan. 2017.

[3] Y. Zhang, R. Xiong, H. He, and W. Shen, "A lithium-ion battery pack state of charge and state of energy estimation algorithms using a hardware-in-the-loop validation," *IEEE Trans. Power Electron.*, to be published, doi: 10.1109/TPEL.2016. 2603229.

[4] Z. Zhang, H. Gui, D. Gu, Y. Yang, and X. Ren, "A hierarchical active balancing architecture for lithium-ion batteries," *IEEE Trans. Power Electron.*, to be published, doi: 10.1109/TPEL.2016.2575844.

[5] B. Xia, T. Nguyen, J. Yang, and C. Mi, "The improved interleaved voltage measurement method for series connected battery packs," *J. Power Sources*, vol. 334, pp. 12–22, Dec. 2016.

[6] B. Xia and C. Mi, "A fault-tolerant voltage measurement method for series connected battery packs," *J. Power Sources*, vol. 308, pp. 83–96, Mar. 2016.

[7] J. G.-Lozano and E. R. Cadaval, "Battery equalization active methods," *J. Power Sources*, vol. 246, pp. 934–949, Jan. 2014.

[8] G.-L. Javier, R.-C. Enrique, M.-M. M. Isabel, and G.-M. A. Miguel, "A novel active battery equalization control with on-line unhealthy cell detection and cell change decision," *J. Power Sources*, vol. 299, pp. 356–370, Dec. 2015.

[9] C. Pascual and P. T. Krein, "Switched capacitor system for automatic series battery equalization," in *Proc. IEEE Appl. Power Electron. Conf.*, 1997, pp. 848–854.

[10] Y. Ye, K. W. E. Cheng, and Y. P. B. Yeung, "Zero-current switching switched-capacitor zero-voltage-gap automatic equalization system for series battery string," *IEEE Trans. Power Electron.*, vol. 27, no. 7, pp. 3234–3242, Jul. 2012.

[11] A. C. Baughman and M. Ferdowsi, "Double-tiered switched-capacitor battery charge equalization technique," *IEEE Trans. Ind. Electron.*, vol. 55, no. 6, pp. 2277–2285, Jun. 2008.

[12] M.-Y. Kim, C.-H. Kim, Jun-Ho Kim, and Gun-Woo Moon, "A chain structure of switched capacitor for improve cell balancing speed of lithium-ion batteries," *IEEE Trans. Ind. Electron.*, vol. 61, no. 8, pp. 3989–3999, Aug. 2014.

[13] Y. Ye and K. W. E. Cheng, "Modeling and analysis of series-parallel switched-capacitor voltage equalizer for battery/supercapacitor strings," *IEEE J. Emerg. Sel. Topics Power Electron.*, vol. 3, no. 4, pp. 977–983, Dec. 2015.

[14] Y. Ye and K. W. E. Cheng, "An automatic switched-capacitor cell balancing circuit for series-connected battery strings," *Energies*, vol. 9, no. 3, pp. 1–15, Feb. 2016.

[15] Y. Ye, K. W. E. Cheng, Y. C. Fong, X. Xue, and J. Lin, "Topology, modeling and design of switched-capacitor-based cell balancing systems and their balancing exploration," *IEEE Trans. Power Electron.*, to be published, doi: 10.1109/TPEL.2016.2584925.

[16] K. Lee, Y. Chung, C.-H. Sung, and B. Kang, "Active cell balancing of li-ion batteries using LC series resonant circuit," *IEEE Trans. Ind. Electron.*, vol. 62, no. 9, pp. 5491–5501, Sep. 2015.

[17] Y. Shang, C. Zhang, N. Cui, and J. M. Guerrero, "A cell-to-cell battery equalizer with zero-current switching and zero-voltage gap based on quasi-resonant LC converter and boost converter," *IEEE Trans. Power Electron.*, vol. 30, no. 7, pp. 3731–3747, Jul. 2015.

[18] Y. Shang, C. Zhang, N. Cui, K. Sun, and J. M. Guerrero, "A crossed pack-to-cell equalizer based on quasi-resonant LC converter with adaptive fuzzy logic equalization control for series-connected lithium-ion battery strings," in *Proc. IEEE Appl. Power Electron. Conf.*, 2015, pp. 1685–1692.
[19] F. Mestrallet, L. Kerachev, J.-C. Crebier, and A. Collet, "Multiphase interleaved converter for lithium battery active balancing," *IEEE Trans. Power Electron.*, vol. 29, no. 6, pp. 2874–2881, Jun. 2014.
[20] T. H. Phung, A. Collet, and J.-C. Crebier, "An optimized topology for next-to-next balancing of series-connected lithium-ion cells," *IEEE Trans. Power Electron.*, vol. 29, no. 9, pp. 4603–4613, Sep. 2014.
[21] M.-Y. Kim, J.-H. Kim, and G.-W. Moon, "Center-cell concentration structure of a cell-to-cell balancing circuit with a reduced number of switches," *IEEE Trans. Power Electron.*, vol. 29, no. 10, pp. 5285–5297, Oct. 2014.
[22] M. Arias, J. Sebastián, M. Hernando, U. Viscarret, and I. Gil, "Practical application of the wave-trap concept in battery-cell equalizers," *IEEE Trans. Power Electron.*, vol. 30, no. 10, pp. 5616–5631, Oct. 2015.
[23] C. Hua and Y.-H. Fang, "A charge equalizer with a combination of APWM and PFM control based on a modified half-bridge converter," *IEEE Trans. Power Electron.*, vol. 31, no. 4, pp. 2970–2979, Apr. 2016.
[24] M. Uno and A. Kukita, "Double-switch equalizer using parallel-or series-parallel-resonant inverter and voltage multiplier for series-connected supercapacitors," *IEEE Trans. Power Electron.*, vol. 29, no. 2, pp. 812–828, Feb. 2014.
[25] S. Li, C. Mi, and M. Zhang, "A high-efficiency active battery-balancing circuit using multiwinding transformer," *IEEE Trans. Ind. Appl.*, vol. 49, no. 1, pp. 198–207, Jan. 2013.
[26] A. M. Imitiaz and F. H. Khan, "Time shared flyback converter" based regenerative cell balancing technique for series connected li-ion battery strings," *IEEE Trans. Power Electron.*, vol. 28, no. 12, pp. 5960–5975, Dec. 2013.
[27] Y. Chen, X. Liu, Y. Cui, J. Zou, and S. Yang, "A multi-winding transformer cell-to-cell active equalization method for lithium-ion batteries with reduced number of driving circuits," *IEEE Trans. Power Electron.*, vol. 31, no. 7, pp. 4916–4929, Jul. 2016.
[28] S.-H. Park, K.-B. Park, H.-S. Kim, G.-W. Moon, and M.-J. Youn, "Single-magnetic cell-to-cell charge equalization converter with reduced number of transformer windings," *IEEE Trans. Power Electron.*, vol. 27, no. 6, pp. 2900–2911, Jun. 2012.
[29] Y. Ye and K. W. E. Cheng, "Voltage-gap modeling method for single-stage switched-capacitor converters," *IEEE J. Emerg. Sel. Topics Power Electron.*, vol. 2, no. 4, pp. 808–813, Dec. 2014.
[30] Y. Ye and K. W. E. Cheng, "Level-shifting multiple-input switched-capacitor voltage copier," *IEEE Trans. Power Electron.*, vol. 27, no. 2, pp. 828–837, Feb. 2012.
[31] B. Dong, Y. Li, and Y. Han, "Parallel architecture for battery charge equalization," *IEEE Trans. Power Electron.*, vol. 30, no. 9, pp. 4906–4913, Sep. 2015.

Yunlong Shang (S'14) received the B.S. degree in automation from Hefei University of Technology, Hefei, China, in 2008.

Since 2010, he has been working toward the Ph.D. degree in the School of Control Science and Engineering, Shandong University, Shandong, China. In 2015, he received the funding from China Scholarship Council, and became a joint Ph.D. in the Department of Electrical and Computer Engineering, San Diego State University, California, USA. His current research interests include the design and control of battery management systems and battery equalizers, battery modeling, and battery state estimation.

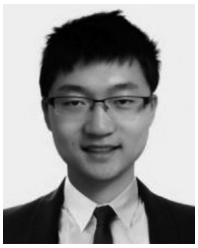

Bing Xia (S'13) received the B.S. degree in mechanical engineering from the University of Michigan, Ann Arbor, MI, USA, in 2012, and the B.S. degree in electrical engineering from Shanghai Jiaotong University, Shanghai, China, in 2012, and the Ph.D. degree in automotive system engineering from the University of Michigan Dearborn, Dearborn, MI, USA, between Winter 2013 and Summer 2015.

Starting from Fall 2015, he is the Ph.D. candidate in the joint Ph.D. program with San Diego State University and University of California, San Diego. His research interests include on batteries, including charging optimization, battery safety, and battery management.

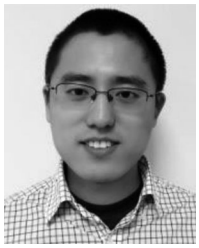

Fei Lu (S'12) received the B.S. and M.S. degrees in electrical engineering both from the Harbin Institute of Technology, Harbin, China, in 2010 and 2012, respectively. He is currently working toward the Ph.D. degree in electrical engineering from the University of Michigan, Ann Arbor, MI, USA.

He is working on the high power and high efficiency capacitive power transfer through an air-gap distance up to 100's of millimeters. He is also working on the application of wide band-gap devices on WPT system. His research interests focuses on wireless power transfer for the application of electric vehicle charging.

Chenghui Zhang (M'14) received the Bachelor's and Master's degrees in automation engineering both from Shandong University of Technology, Jinan, China, in 1985 and 1988,respectively, and the Ph.D. degree in control theory and operational research from Shandong University in 2001.

In 1988, he joined Shandong University, where he is currently a Professor of School of Control Science and Engineering at Shandong University, the Chief Manager of Power Electronic Energy-saving Technology and Equipment Research Center of Education Ministry, a Specially Invited Cheung Kong Scholars Professor by China Ministry of Education, and a Taishan Scholar Special Adjunct Professor. He is also one of State-level candidates of "the New Century National Hundred, Thousand, and Ten Thousand Talent Project," the academic leader of Innovation Team of Ministry of Education, and the chief expert of the National "863" high technological planning. His research interests include optimal control of engineering, power electronics and motor drives, energy-saving techniques, and time-delay systems.

Naxin Cui (M'14) received the B.S. degree in automation from Tianjin University, China, in 1989, and the M.S. and Ph.D. degrees in control theory and control engineering both from Shandong University, Jinan, China, in 1994 and 2005, respectively.

In 1994, she joined Shandong University, where she is currently a Full Professor with the School of Control Science and Engineering. Her current research interests include power electronics, motor drives, automatic control theory and application, and battery energy management system of electric vehicles.

Chunting Chris Mi (S'00–A'01–M'01–SM'03–F'12) received the B.S.E.E. and M.S.E.E. degrees in electrical engineering from Northwestern Polytechnical University, Xi'an, China, and the Ph.D. degree in electrical engineering from the University of Toronto, Toronto, ON, Canada.

He is a Professor and Chair of electrical and computer engineering and the Director of the Department of Energy -funded Graduate Automotive Technology Education Center for Electric Drive Transportation, San Diego State University, San Diego, CA, USA. Prior to joining SDSU, he was with the University of Michigan –Dearborn, Dearborn, MI, USA, from 2001 to 2015. From 2008 to 2011, he was the President and the Chief Technical Officer of 1Power Solutions, Inc. He is the Cofounder of Gannon Motors and Controls LLC and Mia Motors, Inc. He has conducted extensive research and has published more than 100 journal papers. He has taught tutorials and seminars on the subject of HEVs/PHEVs for the Society of Automotive Engineers (SAE), the IEEE, workshops sponsored by the National Science Foundation, and the National Society of Professional Engineers. He has delivered courses to major automotive OEMs and suppliers, including GM, Ford, Chrysler, Honda, Hyundai, Tyco Electronics, A&D Technology, Johnson Controls, Quantum Technology, Delphi, and the European Ph.D. School. He has offered tutorials in many countries, including the U.S., China, Korea, Singapore, Italy, France, and Mexico. He has published more than 100 articles and delivered 30 invited talks and keynote speeches. He has also served as a panelist in major IEEE and SAE conferences. His research interests include electric drives, power electronics, electric machines, renewable-energy systems, and electrical and hybrid vehicles.

Dr. Mi received the "Distinguished Teaching Award" and "Distinguished Research Award" of University of Michigan–Dearborn. He received the 2007 IEEE Region 4 "Outstanding Engineer Award," "IEEE Southeastern Michigan Section Outstanding Professional Award." and the "SAE Environmental Excellence in Transportation (E2T)".